Iterative reconstruction scheme for optical tomography based on the equation of radiative transfer

Alexander D. Klose[a] and Andreas H. Hielscher[b]
State University of New York Health Science Center at Brooklyn, Department of Pathology, Box 25, 450 Clarkson Avenue, Brooklyn, New York 11203

(Received 4 December 1998; accepted for publication 6 May 1999)

We report on the development of an iterative image reconstruction scheme for optical tomography that is based on the equation of radiative transfer. Unlike the commonly applied diffusion approximation, the equation of radiative transfer accurately describes the photon propagation in turbid media without any limiting assumptions regarding the optical properties. The reconstruction scheme consists of three major parts: (1) a forward model that predicts the detector readings based on solutions of the time-independent radiative transfer equation, (2) an objective function that provides a measure of the differences between the detected and the predicted data, and (3) an updating scheme that uses the gradient of the objective function to perform a line minimization to get new guesses of the optical properties. The gradient is obtained by employing an adjoint differentiation scheme, which makes use of the structure of the finite-difference discrete-ordinate formulation of the transport forward model. Based on the new guess of the optical properties a new forward calculation is performed to get new detector predictions. The reconstruction process is completed when the minimum of the objective function is found within a defined error. To illustrate the performance of the code we present initial reconstruction results based on simulated data. © *1999 American Association of Physicists in Medicine.* [S0094-2405(99)01208-0]

Key words: equation of radiative transfer, optical tomography, finite difference, discrete ordinates, turbid media, inverse problems, upwind scheme, adjoint differentiation

I. INTRODUCTION

In recent years optical methods using near-infrared light (NIR) have become increasingly important for noninvasive diagnostics in medicine.[1–3] A major area of interest is optical tomography (OT). This novel imaging modality tries to reconstruct the distribution of optical properties inside an object by using results of light-transmission measurements performed on the circumference. Typically, the properties of interest are the scattering coefficient μ_s, the reduced scattering coefficient $\mu_s' = (1-g)\mu_s$, the absorption coefficient μ_a, or the diffusion coefficient $D = c/(3(\mu_a + \mu_s'))$. The anisotropy factor g is defined as the expectation value of the cosine of the scattering angle θ,[4] and $c = c_{\text{vac}}/n$ is the ratio of the speed of light, c_{vac}, and the refractive index, n, of the medium. Changes in the optical properties are closely related to physiological and pathological changes of different tissues. For example, OT has been used to detect brain hemorrhages,[5–7] to diagnose breast cancer,[8,9] and to investigate rheumatoid arthritis in finger joints.[10–12]

The technology for making light-transmission measurement on human subjects is nowadays readily available.[5,13–16] However, a major challenge remains the development of algorithms that transform these measurements into useful images. Research groups have devised various mathematical methods for solving the reconstruction problem in OT. Commonly applied schemes are modified backprojection methods,[17–19] diffraction tomography,[20–23] perturbation approaches,[24–30] full matrix inversion techniques[31–39] and elliptic system methods.[40,41] All these reconstruction schemes are generally based on the diffusion approximation to the equation of radiative transfer.[42–44] Furthermore, most of the currently available imaging techniques require that the objects to be reconstructed are small perturbations to an otherwise known reference medium. For a more detailed review of state-of-the-art reconstruction schemes, see, for example, Refs. 45 and 46.

Recently, increasing attention has been paid to gradient-based iterative image reconstruction (GIIR) methods, which overcome the limitations of small perturbations.[46–50] These iterative schemes consist of three major parts: (1) a diffusion forward model that uses the diffusion equation to predict the detector readings based on a given spatial distribution of optical properties, (2) an objective function Φ that compares the predicted with measured signals, and (3) an updating scheme that uses the gradient of the objective function with respect to the optical properties to provide optical parameters for subsequent forward calculations. Our group reported on a particular scheme[46] that uses adjoint differentiation techniques to calculate the gradient of the objective function and employs a gradient-based line-minimization technique to generate updated optical parameters. We demonstrated the successful reconstruction of two-dimensional (2D) slices through the brain and simple two- and three-dimensional tissue–phantom systems.

All of the currently existing reconstruction schemes, including the GIIR algorithms, are based on the diffusion approximation to the equation for radiative transfer. This approximation is only valid for highly scattering media with

$\mu_s' \gg \mu_a$ and large source–detector pair separation. Thus, this model fails if it is applied to highly absorbing media where the reduced scattering coefficient μ_s' is similar or smaller than the absorption coefficient μ_a. Furthermore, recent studies suggest that diffusion theory fails to accurately describe light propagation in voidlike regions.[51–53] These low scattering and low absorbing areas are present in the cerebrospinal fluid of the brain, the synovial fluid of human finger joints, or the amniotic fluid in the female uterus. Examples for highly absorbing regions in the body are hematoma or liver tissue. For these cases it is highly desirable to have a reconstruction code that is based on the theory of radiative transfer.

Several researchers have already worked on the inverse problem concerning the equation of radiative transfer. A majority of these studies deal with plane-parallel media. For this geometry time-dependent and time-independent solutions have been provided for media that are either spatially homogeneous or nonhomogeneous and have source and detectors either inside or outside the medium.[54–56] Non-plane-parallel configurations were considered only by a few scientists. Larsen[57,58] reports on a method to solve the time-independent inverse transport problem for optically thin media. Elliott[59] found a solution for a weakly absorbing medium with a point source, but did not present actual reconstructions. Wang and Ueno[60] established a theoretical procedure for estimating the two-dimensional distribution of the ground albedo of the earth by measurements made outside the atmosphere. Aronson *et al.*[61] and Chang *et al.*[62] used a Monte-Carlo solution of the adjoint transport equation. To locate discrete absorbers in highly scattering media from tomographic data, Aronson *et al.* applied a backprojection method while Chang *et al.* used a perturbation theory approach. A detailed discussion of most of these methods has been given by McCormick.[63–65] What is still missing is an image reconstruction scheme that efficiently provides the spatial distribution of tissue optical properties for a generally heterogeneous medium given external sources and detector readings obtained on the surface of the medium.

In this work we present a gradient-based iterative reconstruction algorithm for OT that uses the equation of radiative transfer as a forward model. We will first describe the implementation of an upwind scheme for the solution of the equation of radiative transfer. This is followed by the derivation of an adjoint differentiation scheme for the transport equation. This allows an efficient calculation of the gradient of an objective function with respect to the optical parameters. As in our diffusion GIIR algorithm,[46] this gradient is used in a line minimization scheme to find the minimum of the objective function. Finally, we will present and discuss some initial reconstruction results from simulated data for media with varying scattering coefficients.

II. IMAGE RECONSTRUCTION SCHEME

We employ an iterative reconstruction scheme that has three major elements, similar to the previously developed GIIR code. These elements are a forward model, an objective function, and an updating scheme. The forward model gives a numerical solution of the light distribution inside the object Ω and predicts the energy radiance Ψ_d on the boundary $\partial\Omega$ based on the equation of radiative transfer starting with an initial guess $\mu_0=[\mu_{s,0}(r),\mu_{a,0}(r)]$ of the optical parameters and light source $S(r_s)$ at the positions r_s. A given set of measurements M on the boundary $\partial\Omega$ is compared with the set of the predicted radiances $\Psi_d(\mu_0)$ by defining an objective function ϕ. An optimization technique is used to minimize the objective function ϕ. For this optimization the optical parameters μ_0 are updated using the derivative $d\Phi/d\mu$ of the objective function with respect to the optical properties. The gradient is computed by an adjoint differentiation technique, which takes advantage of a well-chosen numerical discretization of the forward model. A new forward calculation is performed based on the new set of optical parameters $\mu_0+\Delta\mu$. The iteration process is finished when the minimum of the objective function is reached within a specified error. At this point the predicted detector readings are identical to the measured detector readings within a given tolerance. The optical parameters, μ, are mapped into a two-dimensional image. In the following sections we describe in detail the three different components and how they work together to yield a reconstructed image of the optical properties.

A. Forward transport model

We use the equation of radiative transfer as a forward model that predicts the detector readings. This integro-differential equation is usually derived by considering energy conservation in a small volume,[43,66] and can be written for the two-dimensional time-dependent case as

$$\frac{1}{c}\frac{\partial\Psi(\mathbf{r},\omega,t)}{\partial t} = S(\mathbf{r},\omega,t) - \omega\cdot\nabla\Psi(\mathbf{r},\omega,t) - (\mu_a+\mu_s)\Psi(\mathbf{r},\omega,t) + \mu_s\int_0^{2\pi} p(\omega,\omega')\Psi(\mathbf{r},\omega',t)\,d\omega'. \quad (1)$$

Here $\mathbf{r}$ is the position vector and ω a unit vector pointing in the direction of photon propagation. $\Psi(\mathbf{r},\omega,t)$ is the energy radiance in units of $\mathrm{W\,cm^{-2}\,sr^{-1}}$. The source term $S(\mathbf{r},\omega,t)$ represents power injected into a solid angle centered on ω in a unit volume at $\mathbf{r}$. The phase function $p(\omega,\omega')$ describes the probability that during a scattering event a photon with direction ω' is scattered into the direction ω.

To solve this equation we use a discrete-ordinate, finite-difference method with vacuum boundary condition, which assumes that the incoming flux on the boundary is zero ($\Psi(\mathbf{r}_b,\omega\cdot\mathbf{n}<0)=0$, where $\mathbf{r}_b$ is a position on the boundary and $\mathbf{n}$ is an outward normal on the boundary).[67–70] In this scheme the integral term in Eq. (1) is replaced by a quadrature formula that uses a finite set of K angular directions ω_k with $k=1,...,K$. This yields a set of K coupled ordinary differential equations for the angular-dependent radiance $\Psi_k(\mathbf{r},t)=\Psi(\mathbf{r},\omega_k,t)$ in the directions ω_k. The coupling term is the internal source term $\mu_s\sum_{k'=1}^{K} a_{k'}p(\omega_{k'},\omega_k)\Psi(\mathbf{r},\omega_{k'},t)$. The parameter $a_{k'}$ is a

weighting factor and depends on the chosen quadrature formula. In this work we apply the *extended trapezoidal rule*.[71] After the angular discretization we obtain

$$\frac{1}{c}\frac{\partial \Psi_k(\mathbf{r},t)}{\partial t} = S_k(\mathbf{r},t) - \omega_k \cdot \nabla \Psi_k(\mathbf{r},t) - (\mu_a + \mu_s)\Psi_k(\mathbf{r},t) + \mu_s \sum_{k'=1}^{K} a_{k'} p_{kk'} \Psi_{k'}(\mathbf{r},t). \tag{2}$$

Additionally, the spatial variable $\mathbf{r}$ needs to be discretized. The domain Ω is subdivided into a set of MN cells defined by a spatial mesh with M points on the x coordinate and N points on the y coordinate. The mesh size along the x axis is Δx and along the y axis is Δy. The angular radiance for the direction ω_k at the grid point (ij) at the position $r=(x_i,y_j)$ is represented by $\Psi_{kij}(x)=\Psi_k(x_i,y_j,t)$. The angular direction ω_k can be expressed in Cartesian coordinates with $\xi_k = e_x \cdot \omega_k = \cos\omega_k$ and $\eta_k = e_y \cdot \omega_k = \sin\omega_k$. The transport equation can now be written as

$$\frac{1}{c}\frac{\partial \Psi_k(x_i,y_j,t)}{\partial t} = S_k(x_i,y_j,t) - \xi_k \frac{\partial \Psi_k(x_i,y_j,t)}{\partial x} - \eta_k \frac{\partial \Psi_k(x_i,y_j,t)}{\partial y} - (\mu_a+\mu_s)\Psi_k(x_i,y_j,t) + \mu_s \sum_{k'=1}^{K} a_{k'} p_{kk'} \Psi_{k'}(x_i,y_j,t). \tag{3}$$

Finally, the spatial derivatives have to be replaced with a finite-difference scheme. This can be done in a variety of ways.[72–75] In this work we use an upwind-difference scheme[76] because it supplies the adequate numerical framework for the gradient calculation performed by the adjoint differentiation, which we are going to describe later. The upwind differencing depends on the direction ω_k of the angular-dependent radiance Ψ_k. Thus, the set of all angular directions ω_k are subdivided into four quadrants and we get four different difference formulas for the radiance Ψ_k:

$$\text{(I)}\quad \xi_k>0, \eta_k>0: \frac{d\Psi}{dx} \approx \frac{\Psi_{i,j}-\Psi_{i-1,j}}{\Delta x}, \quad \frac{d\Psi}{dy} \approx \frac{\Psi_{i,j}-\Psi_{i,j-1}}{\Delta y}, \tag{4a}$$

$$\text{(II)}\quad \xi_k<0, \eta_k>0: \frac{d\Psi}{dx} \approx \frac{\Psi_{i+1,j}-\Psi_{i,j}}{\Delta x}, \quad \frac{d\Psi}{dy} \approx \frac{\Psi_{i,j}-\Psi_{i,j-1}}{\Delta y}, \tag{4b}$$

$$\text{(III)}\quad \xi_k>0, \eta_k<0: \frac{d\Psi}{dx} \approx \frac{\Psi_{i,j}-\Psi_{i-1,j}}{\Delta x}, \quad \frac{d\Psi}{dy} \approx \frac{\Psi_{i,j+1}-\Psi_{i,j}}{\Delta y}, \tag{4c}$$

$$\text{(IV)}\quad \xi_k<0, \eta_k<0: \frac{d\Psi}{dx} \approx \frac{\Psi_{i+1,j}-\Psi_{i,j}}{\Delta x}, \quad \frac{d\Psi}{dy} \approx \frac{\Psi_{i,j+1}-\Psi_{i,j}}{\Delta y}. \tag{4d}$$

For example, for case I the discretized transport equation is given by

$$\frac{1}{c}\frac{\partial \Psi_{i,j,k}(t)}{\partial t} = S_{i,j,k}(t) - \xi_k \frac{\Psi_{i,j,k}(t)-\Psi_{i-1,j,k}(t)}{\Delta x} - \eta_k \frac{\Psi_{i,j,k}(t)-\Psi_{i,j-1,k}(t)}{\Delta y} - (\mu^a_{i,j}+\mu^s_{i,j})\Psi_{i,j,k}(t) + \mu^s_{i,j} \sum_{k'=1}^{K} a_{k'} p_{kk'} \Psi_{i,j,k'}(t). \tag{5}$$

The time discretization is performed using *forward Euler differencing*:[71]

$$\frac{\partial \Psi}{\partial t} \approx \frac{\Psi^{n+1}-\Psi^n}{\Delta t}, \quad n=1,\ldots,n_{\max}. \tag{6}$$

Considering an explicit upwind scheme, we get for case I

$$\Psi^{n+1}_{i,j,k} = \Psi^n_{i,j,k} + c\Delta t S^n_{i,j,k} - c\Delta t \xi_k \frac{\Psi^n_{i,j,k}-\Psi^n_{i-1,j,k}}{\Delta x} - c\Delta t \eta_k \frac{\Psi^n_{i,j,k}-\Psi^n_{i,j-1,k}}{\Delta y} - c\Delta t(\mu^a_{i,j}+\mu^s_{i,j})\Psi^n_{i,j,k} + c\Delta t \mu^s_{i,j} \sum_{k'=1}^{K} a_{k'} p_{kk'} \Psi^n_{i,j,k'}. \tag{7}$$

Analog expression can be found for the other cases II–IV. This explicit upwind scheme is conditionally stable for $\Delta t \leqslant \Delta x/2c$.[76] The steady-state solution is obtained by assuming a time-independent source, $S(t)=S_0$, and iterating the solution until $(U^{n+1}-U^n)<\varepsilon$, with ε being the termination parameter to be defined by the user. At this equilibrium all time derivatives are vanished and we get a solution of the time-independent equation of radiative transfer.

It is important to note that the difference equations of all quadrants can be written as matrix formula and it follows with Ψ and S as $MNK\times 1$ vectors and B and T as $MNK \times MNK$ matrices:

$$\Psi^{n+1} = (B+T)\Psi^n + S. \tag{8}$$

The vectors Ψ of the radiance and S of the external source strength are ordered as follows:

$$\Psi = (\Psi_{111},\Psi_{112},\ldots,\Psi_{121},\Psi_{122},\ldots,\Psi_{211},\Psi_{212},\ldots, \Psi_{kij},\ldots,\Psi_{KMN}). \tag{9}$$

The components B_{kij} and T_{kij} can be found in the Appendix. It is crucial for the adjoint derivative calculation that we can write the solution scheme of the forward problem in a form given by Eq. (8). As we will see later, this form allows

efficient calculation of the gradient of the objective function, which needs to be minimized to obtain a reconstructed image.

B. Objective function

We consider the image reconstruction problem in OT as an optimization problem. The measurements are compared to the predicted detector readings by defining an objective function as least-square functional Φ, which depends on the optical properties:

$$\Phi(\mu)=\sum_m \left(\frac{M_m-\Sigma_k \Psi^n_{mk}(\mu)}{\Sigma_k \Psi^n_{mk}(\mu)}\right)^2 \quad \text{with} \quad n=n_{\max}. \tag{10}$$

The objective function is a sum over all source-detector pairs m. We assume that the detector readings M on the boundary are angular independent. Thus, the predicted radiance Ψ had to be summed over all outward-pointing angles k for each detector position. Additional regularization terms could be added to the least-square term,[46] however, they are not considered in this work. A solution of the image reconstruction problem can be assumed if the difference between measured and predicted data is small. Therefore the task becomes now to minimize the objective function.

C. Optimization technique

The minimization of the objective function Φ, can be performed effectively with optimization techniques that use the gradient $d\Phi/d\mu$ of the objective function Φ with respect to the optical properties μ. We use a method that consists of a one-dimensional line search along the direction of the gradient $d\Phi/d\mu$ to find the minimum of the objective function in that direction.[71] Starting with the initial guess μ_0 and two more points, $\mu_1=\mu_0+\Delta\mu$ and $\mu_2=\mu_0+2\Delta\mu$ chosen along the direction of the gradient, function values $\Phi(\mu_0)$, $\Phi(\mu_1)$, and $\Phi(\mu_2)$ are calculated. The largest function value is neglected and a new point μ_3 is defined applying the *golden section rule*.[71] This procedure is repeated until the intervals between these three points become sufficiently small. A parabola is fitted to the points and the minimum $\Phi(\mu_1)$ is estimated. A new gradient $(d\Phi/d\mu)(\mu_1)$ is calculated at the minimum μ_1 and a new line-minimization begins.

To increase the performance of the line search we employ a Polak–Riberie scheme[71] to calculate the conjugate gradient of $(d\Phi/d\mu)(\mu_1)$ at μ_1 and call it $(d\tilde{\Phi}/d\mu)(\mu_1)$. A next minimum μ_{II} is searched along the new conjugate direction $(d\tilde{\Phi}/d\mu)(\mu_1)$. The entire process is repeated until the minimum of Φ in the μ-space is found. The final result is the reconstructed image represented by the distribution μ_N after N one-dimensional line searches.

D. Gradient calculation with adjoint differentiation

To make use of gradient-based optimization techniques we need to calculate the derivative $d\Phi/d\mu$. For optical tomography analytical expressions of the derivatives are, in general, not available and the derivative calculation by difference approximations leads to long computation times. To overcome these limitations we seek to employ adjoint differentiation techniques,[77–79] which computes the derivatives exactly without truncation error at a computational expense comparable to a forward model run.[80] Adjoint differentiation methods compute the derivatives using the forward code in the reverse direction. As we will see, the recursive form of Eq. (8) plays a crucial role in the implementation of the adjoint differentiation technique.

In our approach to optical tomography the adjoint differentiation technique can be formulated as follows. The derivative, $d\Phi/d\mu_k$, of the objective function with respect to the optical parameter, μ_k, for all time steps n applying the chain rule can be written as

$$\frac{d\Phi}{d\mu_k}=\sum_n \left(\frac{d\Phi}{d\mu_k}\right)^n=\sum_n \left(\sum_j \frac{d\Phi}{d\Psi^n_j}\frac{\partial\Psi^n_j}{\partial\mu_k}\right). \tag{11a}$$

We denote all elements of vectors or matrices only with i, j, or k regardless of the meaning as a position (i,j) or angle k. Equation (11a) can also be written for one fixed time step n as

$$\left(\frac{d\Phi}{d\mu_k}\right)^n=\frac{d\Phi}{d\Psi^n_1}\frac{\partial\Psi^n_1}{\partial\mu_k}+\frac{d\Phi}{d\Psi^n_2}\frac{\partial\Psi^n_2}{\partial\mu_k}+\cdots+\frac{d\Phi}{d\Psi^n_j}\frac{\partial\Psi^n_j}{\partial\mu_k}+\cdots, \tag{11b}$$

and we obtain in matrix notation

$$\begin{bmatrix} \frac{d\Phi}{d\mu_1} \\ \frac{d\Phi}{d\mu_2} \\ \cdot \\ \frac{d\Phi}{d\mu_k} \end{bmatrix}^n = \begin{bmatrix} \frac{\partial\Psi^n_1}{\partial\mu_1} & \frac{\partial\Psi^n_2}{\partial\mu_1} & \cdot & \frac{\partial\Psi^n_j}{\partial\mu_1} \\ \frac{\partial\Psi^n_1}{\partial\mu_2} & \frac{\partial\Psi^n_2}{\partial\mu_2} & \cdot & \frac{\partial\Psi^n_j}{\partial\mu_2} \\ \cdot & \cdot & \cdot & \cdot \\ \cdot & \cdot & \cdot & \frac{\partial\Psi^n_j}{\partial\mu_k} \end{bmatrix} \begin{bmatrix} \frac{d\Phi}{d\Psi^n_1} \\ \frac{d\Phi}{d\Psi^n_2} \\ \cdot \\ \frac{d\Phi}{d\Psi^n_j} \end{bmatrix}. \tag{12}$$

Taking the partial derivative with respect to the optical parameters μ_k we get from Eq. (8) for the elements of the matrix in (12)

$$\frac{\partial\Psi^n_j}{\partial\mu_k}=\frac{\partial B_{ji}}{\partial\mu_k}\Psi^{n-1}_i+\frac{\partial T_{ji}}{\partial\mu_k}\Psi^{n-1}_i. \tag{13}$$

[Here we replaced $(n+1)$ by n in Eq. (8) without loss of generality.] The elements $d\Phi/d\Psi^n_j$ of the vector on the right-hand side of Eq. (12) are computed by the adjoint differentiation technique. That means the derivative $d\Phi/d\Psi^n_j$ of the current time step n is calculated in the adjoint or reverse direction using the derivative $d\Phi/d\Psi^{n+1}_i$ of the time step $(n+1)$ by applying the chain rule. Therefore we obtain

$$\frac{d\Phi}{d\Psi^n_j}=\sum_i \frac{d\Phi}{d\Psi^{n+1}_i}\frac{d\Psi^{n+1}_i}{d\Psi^n_j}+\frac{\partial\Phi}{\partial\Psi^n_j} \tag{14a}$$

or

$$\frac{d\Phi}{d\Psi_j^n}=\frac{d\Phi}{d\Psi_1^{n+1}}\frac{d\Psi_1^{n+1}}{d\Psi_j^n}+\frac{d\Phi}{d\Psi_2^{n+1}}\frac{d\Psi_2^{n+1}}{d\Psi_j^n}+\cdots+\frac{d\Phi}{d\Psi_i^{n+1}}\frac{d\Psi_i^{n+1}}{d\Psi_j^n}+\cdots+\frac{\partial\Phi}{\partial\Psi_j^n} \tag{14b}$$

with $d\Phi/d\Psi_j^n=\partial\Phi/\partial\Psi_j^n$ for $n=n_{\max}$. Applying Eq. (10), the partial derivative $\partial\Phi/\partial\Psi_j^n$ in (14a) yields

$$\frac{\partial\Phi}{\partial\Psi^n}=\begin{cases}2\left(\dfrac{M_j-\Sigma_k\Psi_{jk}^n}{\Sigma_k\Psi_{jk}^n}\right)\left(\dfrac{M_j}{(\Sigma_k\Psi_{jk}^n)^2}\right), & n=n_{\max}.\\ 0, \quad n<n_{\max}, \quad j\neq m.\end{cases} \tag{15}$$

The subscript m denotes the detector positions on the boundary and the subscript k denotes the angles. Differentiating Eq. (8) with respect to Ψ_i^n, we obtain

$$\frac{d\Psi_j^{n+1}}{d\Psi_i^n}=B_{ji}+T_{ji}. \tag{16}$$

Taking the transpose of Eq. (16) we obtain

$$\left(\frac{d\Psi_j^{n+1}}{d\Psi_i^n}\right)^T=\frac{d\Psi_i^{n+1}}{d\Psi_j^n}=B_{ij}+T_{ij}. \tag{17}$$

Inserting Eq. (17) into Eq. (14a) we get

$$\frac{d\Phi}{d\Psi_j^n}=\sum_i (B_{ij}+T_{ij})\frac{d\Phi}{d\Psi_i^{n+1}}+\frac{\partial\Phi}{\partial\Psi_j^n}. \tag{18}$$

Once the derivatives $d\Phi/d\Psi_j^n$ are calculated, the gradient of the objective function with respect to the optical parameters is easily obtained by Eqs. (12) and (11a).

III. RESULTS

We initially tested the code for media that vary in the scattering coefficient. Detector readings were generated on the boundary of the object for several source and detector positions by using the transport forward model with an angular discretization of 16 angles. We assumed a time-independent isotropic source in order to produce time-independent simulated measurements. Subsequently, the calculated detector readings were used as input for the reconstruction algorithm. All calculations where done with a LINUX workstation containing a Pentium II 350 MHz processor.

As a first example we reconstructed a simple heterogeneous medium, which consisted of a 2 cm by 2 cm background medium and two objects [Fig. 1(a)]. The two objects had a size of 0.25 cm by 0.25 cm each. The background medium had optical coefficients of $\mu_s=10.0\,\mathrm{cm}^{-1}$, $\mu_a=0.01\,\mathrm{cm}^{-1}$, and $g=0$. Inside the two heterogeneities the scattering coefficients were $\mu_s=12.0\,\mathrm{cm}^{-1}$ and $\mu_s=8.0\,\mathrm{cm}^{-1}$, respectively, while the absorption coefficient and the anisotropy factor were the same as in the background medium. For the simulations we used a 40 by 40 grid resulting in a pixel size of 0.05 cm and 1600 unknown scattering coefficients. In the center of each side of the medium a source was placed, and 96 equally spaced detectors surrounded the medium. Therefore, this configuration yielded a total of 384 source–detector pairs. As an initial guess we assumed a homogeneous medium with the same optical properties as the background medium.

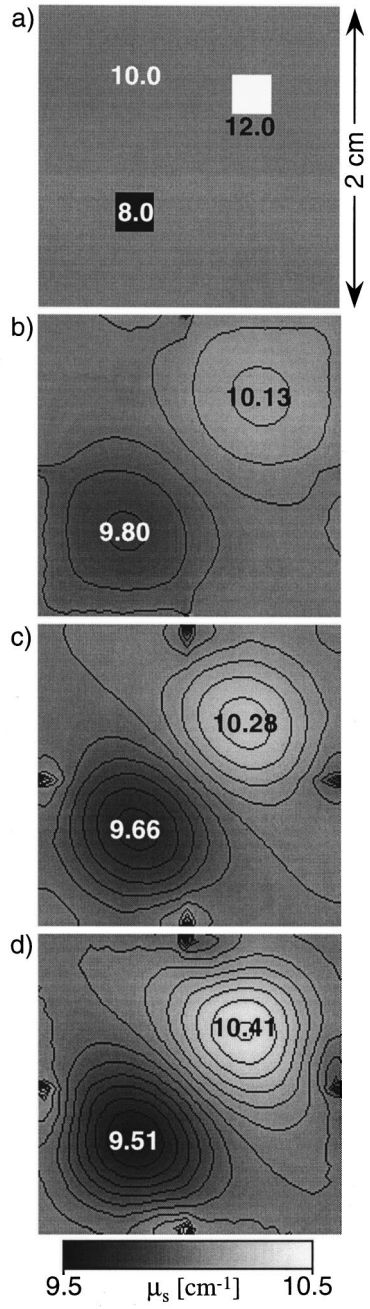

FIG. 1. (a) The original medium of size 2 cm by 2 cm with two inhomogeneities of size 0.25 cm by 0.25 cm. The medium is discretized into 40 by 40 pixels. The optical properties of the isotropic background medium are $\mu_s=10\,\mathrm{cm}^{-1}$, $\mu_a=0.01\,\mathrm{cm}^{-1}$, and $g=0$. The two heterogeneities differ only in the scattering coefficient, which are given by $\mu_s=12.0\,\mathrm{cm}^{-1}$ and $\mu_s=8.0\,\mathrm{cm}^{-1}$. One source is placed in the center of each side and 96 equally space detectors surrounded the medium. Also shown are the reconstructed images (b) after 1 iteration, (c) after 5 iterations, and (d) after 20 iterations.

In Fig. 1(b) the reconstructed images after one iteration can be seen. Figures 1(c) and 1(d) show reconstructions after 5 and 20 iterations. Further iterations resulted in only marginal improvements. The computation time for 20 iterations was approximately 3 h. The positions of the two inhomogeneities could be identified even though the size appeared too large. The absolute values of the scattering coefficients at the positions of the perturbations were underestimated for the object with higher-than-background scattering and overestimated for the object with lower-than-background scattering.

Next we investigated the influence of the number of sources and/or detectors on the reconstruction results. The original object was the same as in the first example [Fig. 2(a)]. The initial guess was a homogeneous medium with the background optical properties. Figures 2(b)–2(d) show the reconstruction after 20 iterations with 4 sources and 16 detectors, 4 sources and 96 detectors, and 16 sources and 96 detectors, respectively. Increasing the number of detectors and sources led to some improvement of the reconstruction results. For example, increasing the number of detectors from 16 to 96 decreased the minimal D value from $D=9.56\,\mathrm{cm^2\,ns^{-1}}$ to $D=9.51\,\mathrm{cm^2\,ns^{-1}}$ (correct $D=8.0\,\mathrm{cm^2\,ns^{-1}}$) and increased the maximal D value from $D=10.37\,\mathrm{cm^2\,ns^{-1}}$ to $D=10.41\,\mathrm{cm^2\,ns^{-1}}$ (correct $D=12.0\,\mathrm{cm^2\,ns^{-1}}$). However, even with 16 sources and 96 detectors absolute values of the scattering coefficients were underestimated by 13.1% for the object with higher-than-background scattering and overestimated by 18.6% for the object with lower-than-background scattering. Further increase in number of sources or detectors only led to marginal (<0.1%) improvements. The computation time approximately doubles if the number of sources is doubled, since for each additional source a full forward calculation becomes necessary. Doubling the number of detectors only leads to a slight increase of computation time, since no additional forward calculations are necessary.

In a third example we varied the mesh size. This time the medium had a background scattering coefficient of $\mu_s=20.0\,\mathrm{cm^{-1}}$ and an absorption coefficient of $\mu_a=0.01\,\mathrm{cm^{-1}}$ [Fig. 3(a)]. The two inhomogeneities had the scattering coefficients of $\mu_s=16.0\,\mathrm{cm^{-1}}$ and $\mu_s=24.0\,\mathrm{cm^{-1}}$, respectively, while μ_a was not changed. Four sources and 40 detectors surrounded the object. We used two different mesh sizes with 0.05 and 0.025 cm. The positions, shape, and optical properties of the heterogeneities could be reconstructed better for the smaller mesh size [Figs. 3(b) and 3(c)]. However, the computation time for 20 iterations increased from 3 h for the 40×40 grid to 12 h for the 80×80 grid.

As a last example, we attempted to reconstruct a highly scattering medium that contained a voidlike ring [Fig. 4(a)]. The medium had a size of 2 cm by 2 cm and was discretized into a 80×80 mesh with $\Delta x=\Delta y=0.025\,\mathrm{cm}$. The background medium had a scattering coefficient of $\mu_s=20.0\,\mathrm{cm^{-1}}$ and an absorption coefficient of $\mu_a=0.01\,\mathrm{cm^{-1}}$. The scattering coefficient of the voidlike ring was decreased by a factor of 40 to $\mu_s=0.5\,\mathrm{cm^{-1}}$, and the absorption coefficient was set to $\mu_a=0.1\,\mathrm{cm^{-1}}$. The anisotropy factor, $g=0$, is constant throughout the medium, therefore $\mu_s=\mu_s'$. The ring had a diameter of 1.45 cm and a thickness of 0.075 cm. Four sources and 40 detectors were placed equally spaced around the object. The time-independent measurements, which were used as the input data for the reconstructions, were generated by the transport forward model. The subsequent reconstructions were performed with the image reconstruction algorithms based on equation of radiative transfer. Additionally we employed a previously developed diffusion-equation-based reconstruction algorithms.[46] This time-dependent diffusion code was easily adapted to the time-

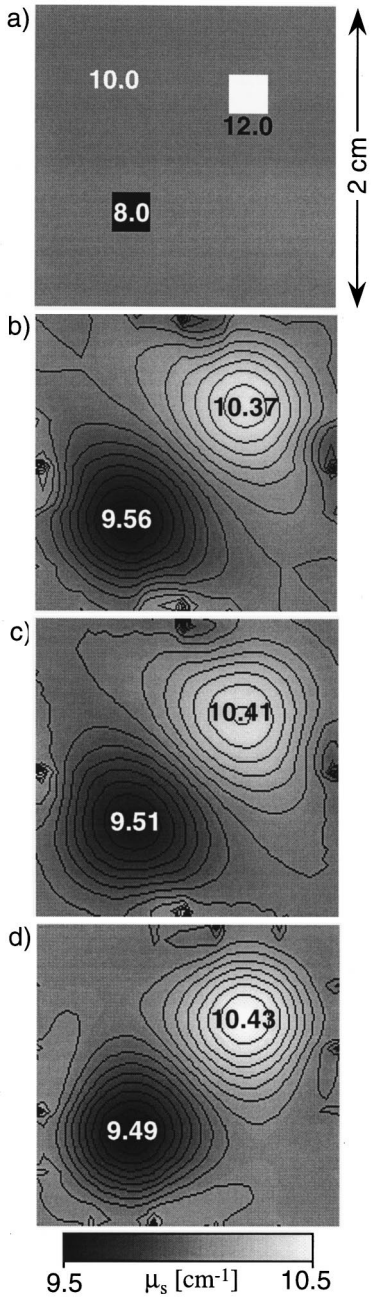

FIG. 2. Influence of the number of sources and detectors on the reconstructed image. (a) The original medium with two inhomogeneities as in Fig. 1(a). The reconstructed images after 20 iterations are shown for (b) 4 sources and 16 detectors, for (c) 4 sources and 96 detectors, and for (d) 16 sources and 96 detectors.

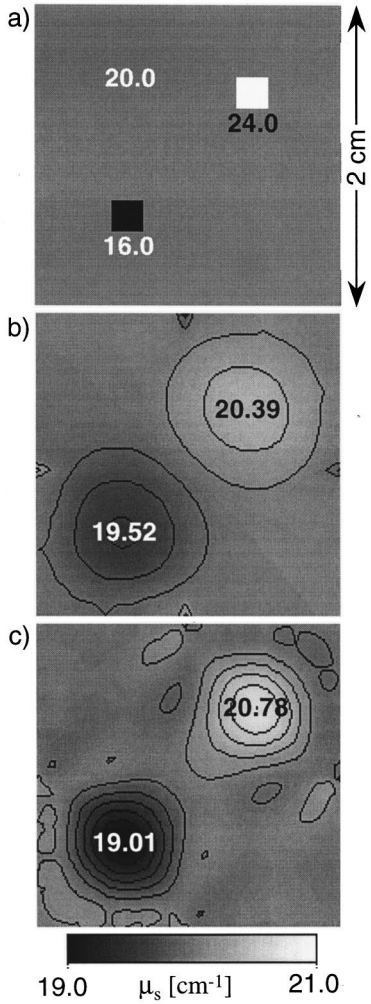

FIG. 3. Influence of the mesh size on the reconstruction. (a) The isotropic original medium with background optical properties of $\mu_s = 20.0\ \mathrm{cm}^{-1}$ and $\mu_a = 0.01\ \mathrm{cm}^{-1}$. The two heterogeneities differ in the scattering coefficients, which are given by $\mu_s = 16.0\ \mathrm{cm}^{-1}$ and $\mu_s = 24.0\ \mathrm{cm}^{-1}$, respectively. One source is placed in the center of each side and 40 equally spaced detectors surrounded the medium. The reconstructed images are shown for the mesh sizes of (b) $\Delta x = \Delta y = 0.05$ cm and (c) $\Delta x = \Delta y = 0.025$ cm.

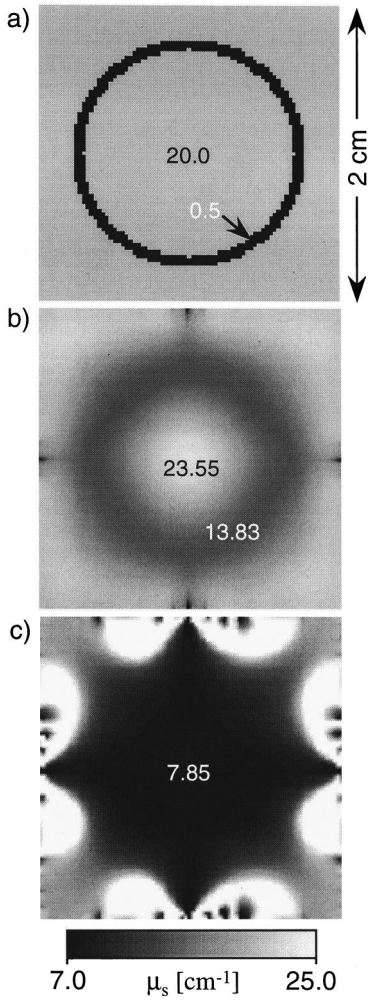

FIG. 4. Comparison of transport-theory-based and diffusion-theory-based image reconstruction of voidlike areas. (a) Homogeneous object with an embedded voidlike circle. The optical properties in the voidlike area are $\mu_s = 0.5\ \mathrm{cm}^{-1}$, $\mu_a = 0.1\ \mathrm{cm}^{-1}$, and $g = 0$. The optical properties of the background medium are $\mu_s = 20.0\ \mathrm{cm}^{-1}$, $\mu_a = 0.01\ \mathrm{cm}^{-1}$, and $g = 0$. The medium is surrounded by 4 sources and 40 detectors, which are equally spaced. The medium is discretized into 80 by 80 pixels, with $\Delta x = \Delta y = 0.025$ cm. The reconstructed images are shown (b) based on theory of radiative transfer after 20 iterations, which take approximately 12 h to compute and (c) based on diffusion theory after 50 iterations, which take approximately 4 h to compute.

independent case by assuming a time-independent source term. For the diffusion reconstruction we generated detector readings with the diffusion forward model. The initial guess for all reconstructions was homogeneous medium with $\mu_s = 20\ \mathrm{cm}^{-1}$.

The reconstructed image based on the transport theory [Fig. 4(b)] clearly shows a ring with a decreased scattering coefficient, even though the absolute value of $\mu_s = 13.83\ \mathrm{cm}^{-1}$ is much too large. This can mainly be attributed to the large initial guess, which is 40 times larger than the actual value in the ring region. The scattering coefficient in the area surrounded by the voidlike ring could be reconstructed within an error of 17.75%.

On the other hand, the reconstruction code based on the diffusion model completely fails to recover either the ring structure or the absolute values of scattering coefficients [Fig. 4(c)]. The voidlike ring and the surrounded center of the medium cannot be distinguished. The diffusion-reconstructed image shows a decreased scattering coefficient in the middle of the object. This is in agreement with earlier experimental and theoretical findings, where it was shown that the diffusion theory predicts that light is channeled in voidlike structures within highly scattering media.[51–53] This means that less light enters into areas enclosed by voidlike regions when the diffusion equation rather than the equation of radiative transfer is used. The light finds a ''short-cut'' around the center region and it appears that the medium has a low scattering coefficient. These results underline the importance of the correct model in reconstruction schemes. A more detailed experimental and theoretical investigation that explores the exact limits of the diffusion model in optical tomography is beyond the scope of this study, but will be treated in future works.

IV. SUMMARY AND OUTLOOK

We have developed an image reconstruction algorithm for time-independent optical tomography that is based on the equation of radiative transfer. Detector readings are predicted by a finite-difference, discrete-ordinate transport code, which employs an upwind scheme. An objective function is defined that compares the predicted with actual detector readings. The minimum of this objective function is determined with a gradient-based line-minimization scheme. For the gradient calculation we employ an adjoint differentiation scheme that makes use of the structure of the transport forward code.

The new image reconstruction algorithm could qualitatively estimate the distribution of the scattering coefficients of simple heterogeneous media. The positions of heterogeneities could be determined with high accuracy, while the absolute values of scattering coefficients were underestimated for objects with higher-than-initial-guess scattering coefficient and overestimated for the object with lower-than-initial-guess scattering coefficient. The image quality could be slightly increased by an increase in the number of sources and detectors. Furthermore, we observed that better reconstructions can be obtained with smaller mesh sizes. The disadvantage of more sources and smaller mesh sizes is the prolonged computation time. Finally, we showed that, unlike diffusion-equation-based algorithms, the transport-equation-based code can find low-scattering, voidlike regions in dense optical media.

Further work has to be done to test and improve the code. The inclusion of absorption reconstruction is straightforward since the equation for the gradient calculation applies for both the μ_s and μ_a. However, the problem of cross-talk between simultaneous μ_s and μ_a reconstruction, as observed already in diffusion-equation-based reconstruction algorithms,[47,81] needs to be evaluated. Furthermore, the influence of nonisotropic phase functions with $g \neq 0$ will be an important issue. This is related to the problem of the optimal number of angles in the angular discretization. Besides increasing the number of sources and decreasing the mesh size, improved reconstruction results may be obtained by time- or frequency-domain formulations of the problem.

There are various ways of increasing the speed of the reconstruction. For example, each forward calculation could be performed on a different processor leading to a parallelization of the code. The one-dimensional line search can be accelerated using different optimization techniques as quasi-Newton search or the Broyden–Fletcher–Goldfarb–Shanno (BFGS) update.[82] Furthermore, the proper use of prior information in the initial guess as well as in regularization schemes could not only shorten the convergence time but also leads to improved accuracy in the reconstruction.

Finally, the accuracy of the upwind difference scheme, which is only a first-order finite-difference approximation, should be compared with high-order finite-difference approximations such as the diamond difference scheme[75] or centered space difference scheme.[74] Diamond difference schemes, furthermore, have the advantage that acceleration methods exist that lead to reduced forward computation times.[83,84] On the other hand, the structure of these codes complicates the gradient calculation and the development of efficient adjoint differentiation techniques has been elusive so far.

ACKNOWLEDGMENTS

This work was supported in part by The Whitaker Foundation, Grant No. 98-0244: Model-based iterative reconstruction techniques for optical tomography, and the Dean's Office of the College of Medicine at the State University of New York Health Science Center Brooklyn (SUNY HSCB). Furthermore, the authors would like to thank Dr. Raymond Alcouffe, Los Alamos National Laboratory, for many useful discussions concerning numerical methods in radiative transfer theory, and Dr. Randall L. Barbour, SUNY HSCB, for providing computational resources.

APPENDIX: MATRIX COMPOSITION

The matrix B is split up into four submatrices for each quadrant of the angles with $B_{\mathrm{I}}: \xi_k > 0, \eta_k > 0$, $B_{\mathrm{II}}: \xi_k < 0, \eta_k > 0$, $B_{\mathrm{III}}: \xi_k < 0, \eta_k < 0$, $B_{\mathrm{IV}}: \xi_k > 0, \eta_k < 0$:

$$B = \begin{pmatrix} B_{\mathrm{I}} & & & 0 \\ & B_{\mathrm{II}} & & \\ & & B_{\mathrm{III}} & \\ 0 & & & B_{\mathrm{IV}} \end{pmatrix},$$

$$B_q = \begin{pmatrix} B_{q_1} & 0 & 0 & \cdot & \cdot & \cdot \\ 0 & B_{q_2} & 0 & \cdot & \cdot & \cdot \\ 0 & 0 & \cdot & \cdot & \cdot & \cdot \\ \cdot & \cdot & \cdot & \cdot & \cdot & \cdot \\ \cdot & \cdot & \cdot & \cdot & \cdot & \cdot \\ \cdot & \cdot & \cdot & \cdot & \cdot & B_{q_k} \end{pmatrix}, q \in \{\mathrm{I,II,III,IV}\}.$$

The elements B_{ij} of a submatrix B_{qk}, where q denotes the quadrant, depend on their index k of the angle:

Quadrant I:

$$B_{ij} = 1 - c\Delta t \Delta x^{-1} \xi_k - c\Delta t \Delta y^{-1} \eta_k - c\Delta t(\mu_{ij}^a + \mu_{ij}^s),$$

$$B_{i-1j} = c\Delta t \Delta x^{-1} \xi_k,$$

$$B_{ij-1} = c\Delta t \Delta y^{-1} \eta_k.$$

Quadrant II:

$$B_{ij} = 1 + c\Delta t \Delta x^{-1} \xi_k - c\Delta t \Delta y^{-1} \eta_k - c\Delta t(\mu_{ij}^a + \mu_{ij}^s),$$

$$B_{i+1j} = -c\Delta t \Delta x^{-1} \xi_k,$$

$$B_{ij-1} = c\Delta t \Delta y^{-1} \eta_k.$$

Quadrant III:

$$B_{ij} = 1 + c\Delta t \Delta x^{-1} \xi_k + c\Delta t \Delta y^{-1} \eta_k - c\Delta t(\mu_{ij}^a + \mu_{ij}^s),$$

$$B_{i+1j} = -c\Delta t \Delta x^{-1} \xi_k,$$

$$B_{ij+1} = -c\Delta t \Delta y^{-1} \eta_k.$$

Quadrant IV:

$$B_{ij} = 1 - c\Delta t\Delta x^{-1}\xi_k + c\Delta t\Delta y^{-1}\eta_k - c\Delta t(\mu_{ij}^a + \mu_{ij}^s),$$

$$B_{i-1j} = c\Delta t\Delta x^{-1}\xi_k,$$

$$B_{ij+1} = -c\Delta t\Delta y^{-1}\eta_k.$$

The matrix T denotes the internal source terms of the transport equation contributed by scattering. The elements T_{kij} are $T_{kij} = c\Delta t\mu_{ij}^s hp$ with the step size $h = 2\pi K^{-1}$ of the *extended trapezoidal rule*.[71] The phase function of the isotropic case is $p = (2\pi)^{-1}$.

[a]Electronic mail: aklose@netmail.hscbklyn.edu
[b]Electronic mail: ahielscher@netmail.hscbklyn.edu

[1]G. Müller, B. Chance, R. Alfano, S. Arridge, J. Beuthan, E. Gratton, M. Kaschke, B. Masters, S. Svanberg, and P. van der Zee, *Medical Optical Tomography: Functional Imaging and Monitoring*, SPIE Institutes for Advanced Optical Technologies Series, Vol. IS11 (1993).
[2]*Advances in Optical Imaging and Photon Migrations*, edited by R. R. Alfano and J. G. Fujimoto, OSA Trends in Optics and Photonics Series, Vol. 2 (Optical Society of America, Washington, DC, 1996).
[3]*Optical Tomography and Spectroscopy of Tissue: Theory, Instrumentation, Model Human Studies II*, edited by B. Chance and R. R. Alfano, SPIE Proc. 2979 (The International Society for Optical Engineering, Bellingham, WA, 1997).
[4]*Optical-Thermal Response of Laser-Irradiated Tissue*, edited by A. J. Welch and M. J. C. van Gemert (Plenum, New York, 1995).
[5]J. P. Vanhouten, D. A. Benaron, S. Spilman, and D. K. Stevenson, ''Imaging brain injury using time-resolved near-infrared light scanning,'' Pediatr. Res. **39**, 470–476 (1996).
[6]D. A. Benaron, J. P. Vanhouten, W. Cheong, E. L. Kermit, and R. A. King, ''Early clinical results of time-of-flight optical tomography in a neonatal intensive care unit,'' Proc. SPIE **2389**, 582–596 (1995).
[7]S. P. Gopinath, C. S. Robertson, C. F. Contant, R. K. Narayan, R. G. Grossman, and B. Chance, ''Early detection of delayed traumatic intracranial hematomas using near-infrared spectroscopy;'' J. Neurosurg. **83**, 438–444 (1995).
[8]S. Nioka, Y. Yung, M. Shnall, S. Zhao, S. Orel, C. Xie, B. Chance, and L. Solin, ''Optical imaging of breast tumor by means of continuous waves,'' Adv. Exp. Med. Biol. **411**, 227–232 (1997).
[9]M. A. Franceschini, K. T. Moesta, S. Fantini, G. Gaida, E. Gratton, H. Jess, W. W. Mantulin, M. Seeber, P. M. Schlag, and M. Kaschke, ''Frequency-domain techniques enhance optical mammography: initial clinical results,'' Proc. Natl. Acad. Sci. USA **94(12)**, 6468–6473 (1997).
[10]J. Beuthan, V. Prapavat, R.-D. Naber, O. Minet, and G. Müller, ''Diagnosis of inflammatory rheumatic diseases with photon density waves,'' Proc. SPIE **2676**, 43–53 (1996).
[11]A. Klose, V. Prapavat, O. Minet, J. Beuthan, and G. Mueller, ''RA diagnostics applying optical tomography in frequency-domain,'' Proc. SPIE **3196**, 194–204 (1997).
[12]A. D. Klose, A. H. Hielscher, K. M. Hanson, and J. Beuthan, ''Three-dimensional optical tomography of a finger joint model for diagnostic of rheumatoid arthritis,'' Proc. SPIE Int. Soc. Opt. Eng. **3566**, 151–160 (1998).
[13]K. Wells, J. C. Hebden, F. E. W. Schmidt, and D. T. Delpy, ''The UCL multichannel time-resolved system for optical tomography,'' Proc. SPIE **2979**, 599–607 (1997).
[14]H. Jess, H. Erdl, K. T. Moesta, S. Fantini, M. A. Franceschini, E. Gratton, and M. Kaschke, ''Intensity modulated breast imaging: Technology and clinical pilot study results,'' in *Advances in Optical Imaging and Photon Migration*, OSA Trends in Optics and Photonics, Vol. II, edited by R. R. Alfano and J. G. Fujimoto (Optical Society of America, Washington, DC, 1996), pp. 126–129.
[15]M. Miwa and Y. Ueda, ''Development of time-resolved spectroscopy system for quantitative noninvasive tissue measurement,'' Proc. SPIE **2389**, 142–149 (1995).
[16]S. Fantini, M. A. Franceschini, J. S. Maier, S. A. Walker, B. Barbieri, and E. Gratton, ''Frequency domain multi-channel optical detector for noninvasive tissue spectroscopy and oximetry,'' Opt. Eng. **34**, 32–42 (1995).
[17]D. A Benaron, D. C. Ho, S. Spilman, J. P. van Houten, and D. K. Stevenson, ''Non-recursive linear algorithms for optical imaging in diffusive media,'' in *Advances in Experimental Medicine & Biology: Oxygen Transport to Tissue XVI* (Plenum, New York, 1994), pp. 215–222.
[18]S. A. Walker, S. Fantini, and E. Gratton, ''Image reconstruction by back-projection from frequency domain optical measurements in highly scattering media,'' Appl. Opt. **36**, 170–179 (1997).
[19]S. B. Colak, D. G. Papaioannou, G. W. 't Hooft, M. B. van der Mark, H. Schomberg, J. C. J. Paasschens, J. B. M. Melissen, and N. A. A. J. van Asten, ''Tomographic image reconstruction from optical projections in light-diffusing media,'' Appl. Opt. **36**, 180–213 (1997).
[20]A. H. Hielscher, F. K. Tittel, and S. L. Jacques, ''Photon density wave diffraction tomography,'' in *OSA Proceedings on Advances in Optical Imaging and Photon Migration*, edited by R. R. Alfano (Optical Society of America, Washington, DC, 1994), Vol. 21, pp. 78–82.
[21]X. D. Li, T Durduran, A. G. Yodh, B. Chance, and D. N. Pattanayak, ''Diffraction Tomography for biomedical imaging with diffuse-photon density waves,'' Opt. Lett. **22**, 573–575 (1997).
[22]C. L. Matson, ''A diffraction tomographic model of the forward problem using diffuse photon density waves,'' Optics Express **1**, 6–11 (1997).
[23]C. L. Matson, N. Clark, L. McMackin, and J. S. Fender, ''Three-dimensional tumor localization in thick tissue with the use of diffuse photon-density waves,'' Appl. Opt. **36**, 214–220 (1997).
[24]R. L. Barbour, H. L. Graber, Y. Wang, J. H. Chang, and R. Aronson, ''A perturbation approach for optical diffusion tomography using continous-wave and time-resolved data,'' in *Medical Optical Tomography*, edited by G. Müller, SPIE Institute for Advanced Optical Technologies (SPIE Optical Engineering, Bellingham, WA, 1993), Vol. IS11, 87–120.
[25]H. L. Graber, J. Chang, R. Aronson, and R. L. Barbour, ''A perturbation model for imaging in dense scattering media: Derivation and evaluation of imaging operators,'' in *Medical Optical Tomography*, edited by G. Müller SPIE Institute for Advanced Optical Technologies (SPIE Optical Engineering, Bellingham, WA, 1993), Vol. IS11, pp. 121–143.
[26]R. L. Barbour, H. L. Graber, J. W. Chang, S. L. S. Barbour, P. C. Koo, and R. Aronson, ''MRI-guided optical tomography: Prospects and computation for a new imaging method,'' IEEE Comput. Sci. Eng. **2**, 63–77 (1995).
[27]Y. Q. Yao, Y. Wang, Y. L. Pei, W. W. Zhu, and R. L. Barbour, ''Frequency-domain optical imaging of absorption and scattering distributions by Born iterative method,'' J. Opt. Soc. Am. A **14**, 325–342 (1997).
[28]J. C. Schottland, J. C. Haselgrove, and J. S. Leigh, ''Photon hitting density,'' Appl. Opt. **32**, 448–453 (1993).
[29]M. A. O'Leary, D. A. Boas, B. Chance, and A. G. Yodh, ''Experimental images of heterogeneous turbid media by frequency-domain diffusion-photon tomography,'' Opt. Lett. **20**, 426–428 (1995).
[30]J. Chang, W. Zhu, Y. Wang, H. Graber, and R. L. Barbour, ''Regularized progressive expansion algorithm for recovery of scattering media from time-resolved data,'' J. Opt. Soc. Am. A **14**, 306–312 (1997).
[31]S. R. Arridge, ''Photon-measurement density functions. Part I: Analytical forms,'' Appl. Opt. **34**, 7395–7409 (1995).
[32]S. R. Arridge and M. Schweiger, ''Photon measurement density functions. Part 2: Finite-element-method calculation,'' Appl. Opt. **34**, 8026–8037 (1995).
[33]M. Schweiger and S. R. Arridge, ''A system for solving the forward and inverse problems in optical spectroscopy and imaging,'' in *Advances in Optical Imaging and Photon Migrations*, OSA Trends in Optics and Photonics Series, Vol. 2, edited by R. R. Alfano and J. G. Fujimoto (Optical Society of America, Washington, DC, 1996), pp. 263–268.
[34]K. D. Paulsen and H. Jiang, ''Spatially varying optical property reconstruction using a finite element diffusion equation approximation,'' Med. Phys. **22**, 691–701 (1995).
[35]K. D. Paulsen and H. Jiang, ''Enhanced frequency domain optical image reconstruction in tissues through total variation minimization,'' Appl. Opt. **35**, 3447–3458 (1996).
[36]H. Jiang, K. D. Paulsen, and U. L. Osterberg, ''Optical image reconstruction using DC data: simulations and experiments,'' Phys. Med. Biol. **41**, 1483–1498 (1996).
[37]H. Jiang, K. D. Paulsen, U. L. Osterberg, B. W. Pogue, and M. S. Patterson, ''Simultaneous reconstruction of optical absorption and scattering maps in turbid media from near-infrared frequency-domain data,'' Opt. Lett. **20**, 2128–2130 (1995).
[38]H. B. Jiang, K. D. Paulsen, U. L. Osterberg, B. W. Pogue, and M. S.

Patterson, ''Optical image reconstruction using frequency domain data: Simulations and experiments,'' J. Opt. Soc. Am. A **13**, 253–266 (1996).
[39]D. Y. Paithankar, A. U. Chen, B. W. Pogue, M. S. Patterson, and E. M. Sevick-Muraca, ''Imaging of fluorescent yield and lifetime from multiply scattered light reemitted from random media,'' Appl. Opt. **36**, 2260–2272 (1997).
[40]M. V. Klibanov, T. R. Lucas, and R. M. Frank, ''A fast and accurate imaging algorithm in optical diffusion tomography,'' Inverse Probl. **13**, 1341–1361 (1997).
[41]T. R. Lucas, M. V. Klibanov, and R. M. Frank, ''Imaging experimental data from optical tomography by the elliptic systems method,'' Proc. SPIE **3171**, 22–33 (1997).
[42]S. Chandrasekhar, *Radiative Transfer* (Oxford U.P., London, 1950) (Dover, New York, 1960).
[43]K. M. Case and P. F. Zweifel, *Linear Transport Theory* (Addison–Wesley, Reading, MA, 1967).
[44]J. J. Duderstadt and W. R. Martin, *Transport Theory* (Wiley, New York, 1979).
[45]S. R. Arridge and J. C. Hebden, ''Optical imaging in medicine: II. Modelling and reconstruction,'' Phys. Med. Biol. **42**, 841–853 (1997).
[46]A. H. Hielscher, A. D. Klose, and K. M. Hanson, ''Gradient-based iterative image reconstruction scheme for time-resolved optical tomography,'' IEEE Trans. Med. Imaging **18**, 262–271 (1999).
[47]S. S. Saquib, K. M. Hanson, and G. S. Cunningham, ''Model-based image reconstruction from time-resolved diffusion data,'' Proc. SPIE **3034**, 369–380 (1997).
[48]A. H. Hielscher, ''Model-based iterative image reconstruction for photon migration tomography,'' Proc. SPIE **3171**, 106–117 (1997).
[49]S. R. Arridge and M. Schweiger, ''A gradient-based optimisation scheme for optical tomography,'' Optics Express **2**, 213–226 (1998).
[50]A. H. Hielscher, A. D. Klose, D. M. Catarious, Jr., and K. M. Hanson, ''Tomographic imaging of biological tissue by time-resolved, model-based, iterative, image reconstruction,'' in *OSA Trends in Optics and Photonics: Advances in Optical Imaging and Photon Migration II*, edited by J. G. Fujimoto (Optical Society of America, Washington, DC, 1998), Vol. 21, pp. 156–161.
[51]A. H. Hielscher, R. E. Alcouffe, and R. L. Barbour, ''Comparison of finite-difference transport and diffusion calculations for photon migration in homogeneous and heterogeneous tissues,'' Phys. Med. Biol. **43**, 1285–1302 (1998).
[52]A. H. Hielscher and R. E. Alcouffe, ''Discrete-ordinate transport simulations of light propagation in highly forward scattering media,'' in *OSA Trends in Optics and Photonics: Advances in Optical Imaging and Photon Migration II*, edited by R. R. Alfano and J. G. Fujimoto (Optical Society of America, Washington, DC, 1998), Vol. 21, pp. 23–28.
[53]M. Firbank, S. R. Arridge, M. Schweiger, and D. T. Delpy, ''An investigation of light transport through scattering bodies with non-scattering regions,'' Phys. Med. Biol. **41**, 767–783 (1996).
[54]L. Fukshansky, N. Fukshansky-Kazarinova, and A. Martinez Remisowsky, ''Estimation of optical properties in a living tissue by solving the inverse problem of the multiflux radiative transfer,'' Appl. Opt. **30**, 3145–3153 (1991).
[55]R. A. Elliott, T. Duracz, N. J. McCormick, and D. R. Emmons, ''Experimental test of a time-dependent inverse radiative transfer algorithm for estimating scattering parameters,'' J. Opt. Soc. Am. A **5**, 366–373 (1988).
[56]R. A. Elliott, T. Duracz, N. J. McCormick, and D. J. Bossert, ''Experimental test of a time-dependent inverse radiative transfer algorithm for estimating scattering parameters: Addendum,'' J. Opt. Soc. Am. A **6**, 603–606 (1989).
[57]E. W. Larsen, ''Solution of the inverse problem in multigroup transport theory,'' J. Math. Phys. **22**, 158–160 (1981).
[58]E. W. Larsen, ''Solution of three dimensional inverse transport problems,'' Transp. Theory Stat. Phys. **17**(2&3), 147–167 (1988).
[59]J. P. Elliott, ''Milne's problem with a point source,'' Proc. R. Soc. London, Ser. A **228**, 424 (1955).
[60]A. P. Wang and S. Ueno, ''An inverse problem in a three-dimensional radiative transfer,'' Astrophys. Space Sci. **155**, 105–111 (1989).
[61]R. Aronson, R. L. Barbour, J. Lubowsky, and H. Graber, ''Application of transport theory to infra-red medical imaging,'' in *Modern Mathematical Methods in Transport Theory*, edited by W. Greenberg and J. Polewczak (Birkhäuser Verlag, Basel, 1991), pp. 64–75.
[62]J. Chang, H. L. Graber, R. L. Barbour, and R. Aronson, ''Recovery of optical cross-section perturbations in dense scattering media by transport-theory-based imaging operators and steady-state simulated data,'' Appl. Opt. **35**, 3963–3978 (1996).
[63]N. J. McCormick, ''Inverse radiative transfer problems: A review,'' Nucl. Sci. Eng. **112**, 185–198 (1992).
[64]N. J. McCormick, ''Methods for solving inverse problems for radiation transport—An update,'' Transp. Theory Stat. Phys. **15**(6&7), 159–772 (1986).
[65]N. J. McCormick, ''Recent developments in inverse scattering transport methods,'' Transp. Theory Stat. Phys. **13**(1&2), 15–28 (1984).
[66]A. Sanchez and N. J. McCormick, ''A Review of neutron transport approximations,'' Nucl. Sci. Eng. **80**, 481–535 (1982).
[67]E. E. Lewis and W. F. Miller, Jr., *Computational Methods of Neutron Transport* (Wiley, New York, 1984).
[68]K. D. Lathrop, ''Discrete-ordinates methods for the numerical solution of the transport equation,'' React. Tech. **15**, 107–134 (1972).
[69]R. D. Richtmyer and K. W. Morton, *Difference Methods for Initial-Value Problems* (Wiley, New York, 1967).
[70]W. F. Ames, *Numerical Methods for Partial Differential Equations* (Academic, New York, 1977).
[71]W. H. Press, S. A. Teukolsky, W. T. Vetterling, and B. P. Flannery, *Numerical Recipes in C* (Cambridge University Press, New York, 1992).
[72]R. E. Alcouffe, E. W. Larsen, W. F. Miller, Jr., and B. R. Wienke, ''Computational efficiency of numerical methods for the multigroup, discrete-ordinates neutron transport equations: the slab geometry case,'' Nucl. Sci. Eng. **71**, 111–127 (1979).
[73]W. H. Reed, ''New difference schemes for the neutron transport equation,'' Nucl. Sci. Eng. **46**, 309–314 (1971).
[74]N. K. Madsen, ''Convergent centered difference schemes for the discrete ordinate neutron transport equations,'' SIAM (Soc. Ind. Appl. Math.) J. Numer. Anal. **12**, 164–176 (1975).
[75]R. E. Alcouffe, ''An adaptive weighted diamond differencing method for three-dimensional xyz geometry,'' Trans. Am. Nucl. Soc. **68**A, 206–212 (1993).
[76]G. Sewell, *The Numerical Solution of Ordinary and Partial Differential Equations* (Academic, San Diego, 1988).
[77]*Automatic Differentiation of Algorithms: Theory, Implementation, and Application*, edited by A. Griewank and G. F. Corliss (SIAM, Philadelphia, 1991).
[78]K. M. Hanson, G. S. Cunningham, and S. S. Saquib, ''Inversion based on complex computational simulations,'' IEEE/EURASIP Workshop on Nonlinear Signal and Image Processing, Mackinac Island, MI, 8–10 September 1997.
[79]A. J. Davies, H. B. Christianson, L. C. W. Dixon, R. Roy, and P. van der Zec, ''Reverse differentiation and the inverse diffusion problem,'' Adv. Eng. Soft. **28**, 217–221 (1997).
[80]W. C. Thacker, ''Automatic differentiation from an oceanographer's perspective,'' in *Automatic Differentiation of Algorithms: Theory, Implementation, and Application*, edited by A. Griewank and G. F. Corliss (SIAM, Philadelphia, 1991), pp. 191–201.
[81]M. Schweiger and S. R. Arridge, ''Optimal data types in optical tomography,'' Proc. of XV International Conference on Information Processing in Medical Imaging, IPMI '97, 9–13 June 1997, Poultney, VT (in press).
[82]D. A. Pierre, *Optimization Theory with Applications* (Dover, New York, 1986).
[83]R. E. Alcouffe, ''A diffusion accelerated S_N transport method for radiation transport on a quadrilateral mesh,'' Nucl. Sci. Eng. **105**, 191–197 (1990).
[84]R. E. Alcouffe, ''Diffusion synthetic acceleration: method for the diamond differenced discrete ordinates equation,'' Nucl. Sci. Eng. **64**, 344–352 (1977).